J Mater Sci (2010) 45:2351–2358
DOI 10.1007/s10853-009-4200-6

Effects of temperature and strain rate on the mechanical properties of lead-free solders

Hongtao Ma

Received: 18 October 2009 / Accepted: 31 December 2009 / Published online: 14 January 2010

Abstract Recently studies of mechanical properties of lead-free solders show that large reductions in stiffness, yield stress, ultimate strength, and strain to failure (up to 35%) were found after 2 months of aging at room temperature. It also shows that the tensile properties of both lead-free solders and Sn–Pb solders tend to become relatively stable after 10 days of aging at room temperature. In this study, in order to minimize any room temperature aging contribution in the investigation of the dependence of temperature and strain rates, all specimens tested were preconditioned after 10 days of aging at room temperature. All tests were conducted under the same conditions. Testing has been performed at three strain rates, 10^{-3}, 10^{-4}, and 10^{-5} s^{-1}, in temperature range from −40 to 150 °C. A linear relationship was found between the temperature and the tensile properties (elastic modulus, yield stress, and ultimate stress), while a power law relationship was found between strain rate and tensile properties. Constitutive models have also been developed based on the experimental data with multiple variables of strain rate and temperature for both lead-free and lead content solders. With the obtained constitutive models, tensile properties of lead-free solders can be predicted at any testing strain rate and temperature.

Introduction

In actual electronic packages, solder joints will be under constant stress at various temperature and strain rates, and due to the high homologous temperature of solder alloys ($T_h > 0.5\ T_m$), the mechanical properties of solder alloys are strongly temperature and strain-rate dependent and their properties will be significantly different under various conditions. The investigation of the dependence on temperature and strain rates is therefore important in order to fully understand the materials behavior of solder alloys, and accurately predict the reliability of solder joints. Hertzberg described that the material strength increases with the testing strain rate, following a form similar to Holloman's equation [1]:

$$\sigma = C\dot{\varepsilon}^m, \tag{1}$$

where m is the strain-rate sensitivity factor or strain hardening exponent, $\dot{\varepsilon}$is the strain rate, C is the material constant, and σ is the stress.

Jones et al. have observed an approximately linear relationship between the strength and temperature [2, 3]:

$$\sigma = -\alpha T + \beta, \tag{2}$$

where α is temperature strengthening coefficient, β is the strength at 0 °C in MPa, and T is the testing temperature in °C. Shi and Pang (co-workers) have observed similar experimental results for a near linear relationship with temperature and a power law relation (Eq. 1) with the strain rate for lead-based solders [4, 5]. Several other studies have also observed similar materials behavior for both Sn–Pb eutectic and lead-free solder alloys [6–9]. Creep modeling studies have also been investigated for other lead-free solders. Raeder et al. have found that steady-state creep of Sn–Bi solders also closely follows hyperbolic sine relation, and higher Bi content appears with higher creep resistance [10]. El-Rehim found that increasing of grain size increases the creep resistance of Sn–Bi lead-free solders [11], the results may be helpful to understand the evolution of creep performance with the evolution of microstructure.

H. Ma (✉)
Auburn University, Auburn, AL 36849, USA
e-mail: hongtaoma@hotmail.com

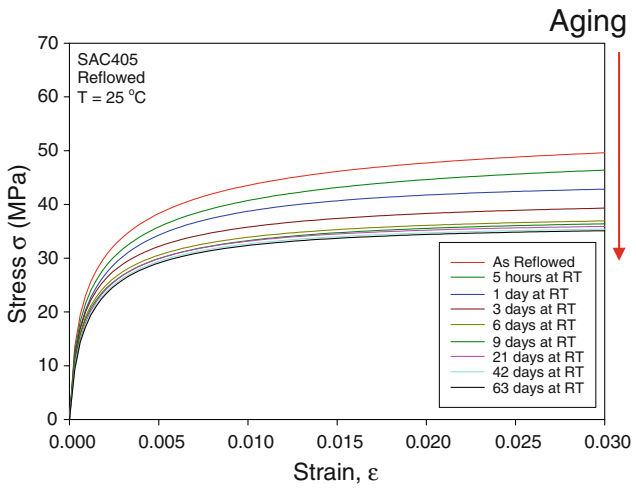

Fig. 1 SAC405 stress–strain curves for various room temperature aging times

Even though there have been various studies on the temperature and strain rate dependence, none of the currently available documented data has documented the possible room temperature contributions in their data, and due to lack of testing standard, the current research data shows large discrepancies in mechanical properties [12]. The recent research shows that room temperature aging effects will dramatically affect the mechanical properties of solder alloys [13]. Any difference in the testing conditions of specimens could seriously affect the accuracy of the data. As shown in Fig. 1, the data show that the tensile strength significantly degrades during room temperature aging up to 2 months of aging time by up to 35% [11]. It also shows that the tensile properties of both SAC405 (Sn–4.0Ag–0.5Cu) lead-free solders and Sn–Pb solders tend to become relatively stable after 10 days of aging at room temperature. In this study on effects of temperature and strain rate, in order to minimize any room temperature aging contribution in the investigation of the dependence of temperature and strain rates, all specimen tested were preconditioned after 10 days of aging at room temperature. All tests were conducted under the same conditions.

Experimental procedure

The solder specimens are originally formed in rectangular cross-section glass tubes using a vacuum suction process. The solder is first melted in a quartz crucible using a pair of circular heating elements (illustrated in Fig. 2). A thermocouple attached on the crucible and a temperature control module is used to direct the melting process. One end of the glass tube is inserted into the molten solder, and suction is applied to the other end via a rubber tube

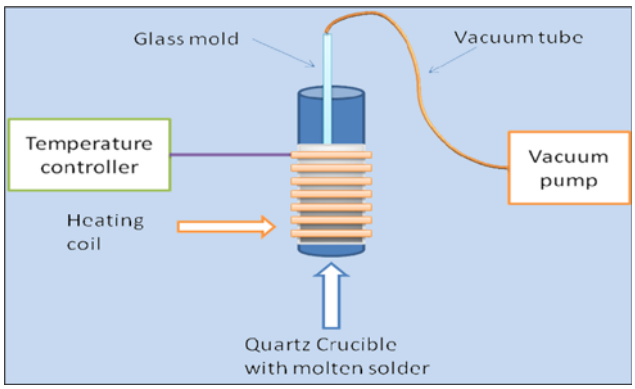

Fig. 2 Illustration of specimen preparation setup

connected to the house vacuum system. The suction forces are controlled through a regulator on the vacuum line so that only a desired amount of solder is drawn into the tube. The specimens are then cooled to room temperature using a user-selected cooling profile.

In order to see the extreme variations possible in the mechanical behavior and microstructure, we are exploring a large spectrum of cooling rates including water quenching of the tubes (fast cooling rate), air cooling with natural and forced convection (slow cooling rates), and controlled cooling using a surface mount technology solder reflow oven. For the reflow oven controlled cooling, the solder in the tubes is first cooled by water quenching, and then sent through a reflow oven (9 zone Heller 1800EXL) to re-melt the solder in the tubes and subject them to the desired temperature profile. Thermocouples are attached to the glass tubes and monitored continuously using a radio-frequency KIC temperature profiling system to ensure that the samples are formed using the desired temperature profile (same as actual solder joints).

Typical glass tube assemblies filled with solder and a final extracted specimen are shown in Fig. 3. For some cooling rates and solder alloys, the final solidified solder samples can be easily pulled from the tubes due to the differential expansions that occur when cooling the low

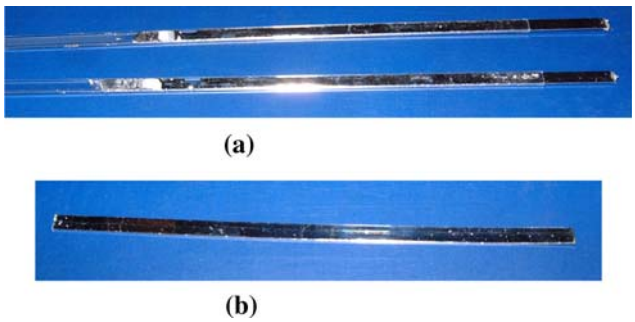

Fig. 3 Solder uniaxial test specimen. **a** Within glass tubes, **b** after extraction

CTE glass tube and higher CTE solder alloy. Other options for more destructive sample removal involve breaking the glass of the glass. The final test specimen dimensions are governed by the useable length of the tube that can be filled with solder, and the cross-sectional dimensions of the hole running the length of the tube. In this work, we formed uniaxial samples with nominal dimensions of 80 × 3 × 0.5 mm. A thickness of 0.5 mm was chosen because it matches the height of typical BGA solder balls. The described sample preparation procedure yielded repeatable samples with controlled cooling profile (i.e., microstructure), oxide free surface, and uniform dimensions. By extensively cross-sectioning several specimens, we have verified that the microstructure of any given sample is consistent throughout the volume of the sample. Typical observed microstructures near the centers of SAC405 and 63Sn–37Pb solder specimens are shown in Fig. 4. The phase size/structure of the final samples can be controlled by the choice of the cooling rate (e.g., faster cooling rate will cause finer the phase structure). In addition, we have established that our method of specimen preparation yields repeatable sample microstructures for a given solidification temperature profile. Samples were inspected using a micro-focus X-ray system to detect flaws (e.g., notches and external indentations) and/or internal voids (non-visible).

A tension/torsion thermo-mechanical test system has been used to test the samples in this study. The system provides an axial displacement resolution of 0.1 μm and a rotation resolution of 0.001°. Testing can be performed in tension, shear, torsion, bending, and in combinations of these loadings, on small specimens such as thin films, solder joints, gold wire, fibers, etc. Cyclic (fatigue) testing can also be performed at frequencies up to 5 Hz. In addition, a universal six-axis load cell was utilized to simultaneously monitor three forces and three moments/torques during sample mounting and testing. Environmental chambers added to the system allow samples to be tested over a temperature range of approximately −75 to +300 °C. A typical recorded tensile stress–strain curve with labeled standard material properties is shown in Fig. 5. In this work, the notation "*E*" is taken to be the effective elastic modulus, which is the initial slope of the stress–strain curve. Since solder is viscoplastic, this effective modulus will be rate dependent, and will approach the true elastic modulus as the testing strain rate approaches infinity. In engineering practice, the value of the elastic modulus obtained from the slope of the stress–strain curve is the static modulus, which is generally referred as the apparent or effective elastic modulus and also includes small inelastic deformations or time-dependent deformations such as creep. The apparent elastic modulus is usually smaller than the dynamic modulus measured by the acoustic or ultrasonic wave method, which largely eliminates the inelastic deformation due to rapid wave propagation. The yield stress σ_Y (YS) is taken to be the standard 0.2% yield stress (upon unloading, the permanent strain is equal to $\varepsilon = 0.002$). Finally, the ultimate tensile strength σ_u (UTS) is taken to be the maximum stress realized in the stress–strain data. In this test, 10 specimens were prepared for each testing conditions. In this study, specimens were aged at room temperature for 10 days before testing. Ten specimens were prepared for each testing condition. All the results represent average of 10 testing results at each condition. Three strain rates were chosen, 10^{-3}, 10^{-4}, and 10^{-5} s^{-1}, and testing temperature ranges from −40 to 150 °C. The stress–strain curve represents multiple average model fit of the 10 test curves as shown in Fig. 6 [13], the peak stress of the model represents the UTS of each condition, the modeled curve only represent average of testing data in *E*, YS, and UTS, the cutoff strains are not the representation of actual strains of each test.

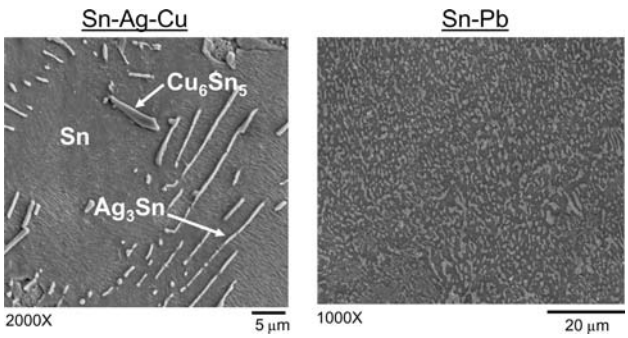

Fig. 4 Typical solder microstructures

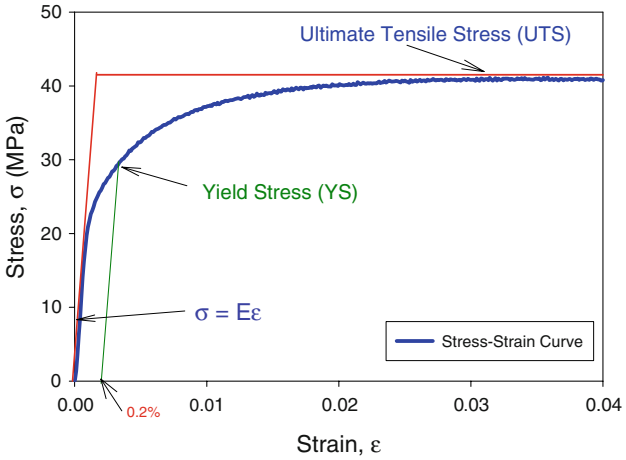

Fig. 5 Typical solder stress–strain curve and material properties

The lead-free solder test results presented in this article were all for samples solidified with the reflowed cooling profile (mimics that seen by actual solder joints during PCB assembly). Finally, in all of the lead-free (SAC)

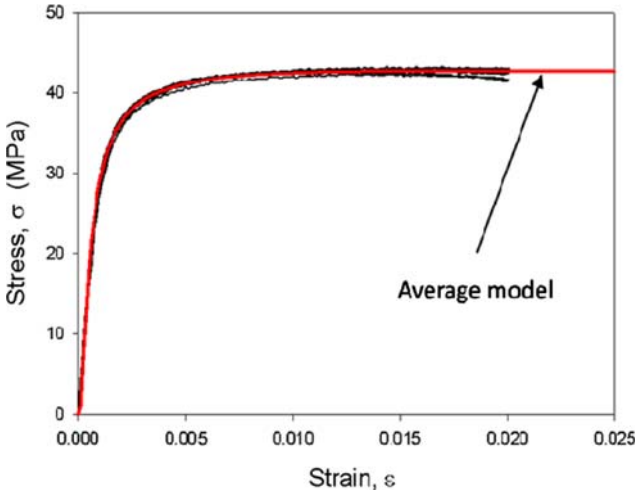

Fig. 6 Average model fit to a typical set of stress–strain curves

testing performed, analogous experiments were also performed with reflowed 63Sn–37Pb eutectic solder samples for comparison purposes.

Results and discussion

Effects of temperature and strain rate on tensile properties

Figure 7 shows the stress–strain curves for SAC405 tested at three strain rates and various temperatures. Figure 8 illustrated the elastic modulus values change with temperature at the three strain rates. The tensile properties were nearly linear with the changing temperature. The tensile properties of the SAC alloy decrease linearly with increasing temperature. The linear relationships of the tensile properties at three strain rates were summarized in Table 1. At a given strain rate, the tensile properties at various temperatures can be predicted with these linear models. Figure 9 illustrates how the tensile properties changes with the changing strain rates at different temperatures. The tensile properties follow a power law relationship. The models are summarized in Table 2, for various temperatures, the tensile properties of the solder alloy can be predicted using the power law models presented in this study at various strain rates. The power constants continue to increase with increasing temperature, which implies that the properties are more sensitive to strain rates at higher temperatures.

Corresponding tensile data for Sn–Pb were also collected at various strain rates and temperatures. Similar as with the SAC alloy, a near linear relationship were also found between key tensile properties (E, UTS, and YS) and

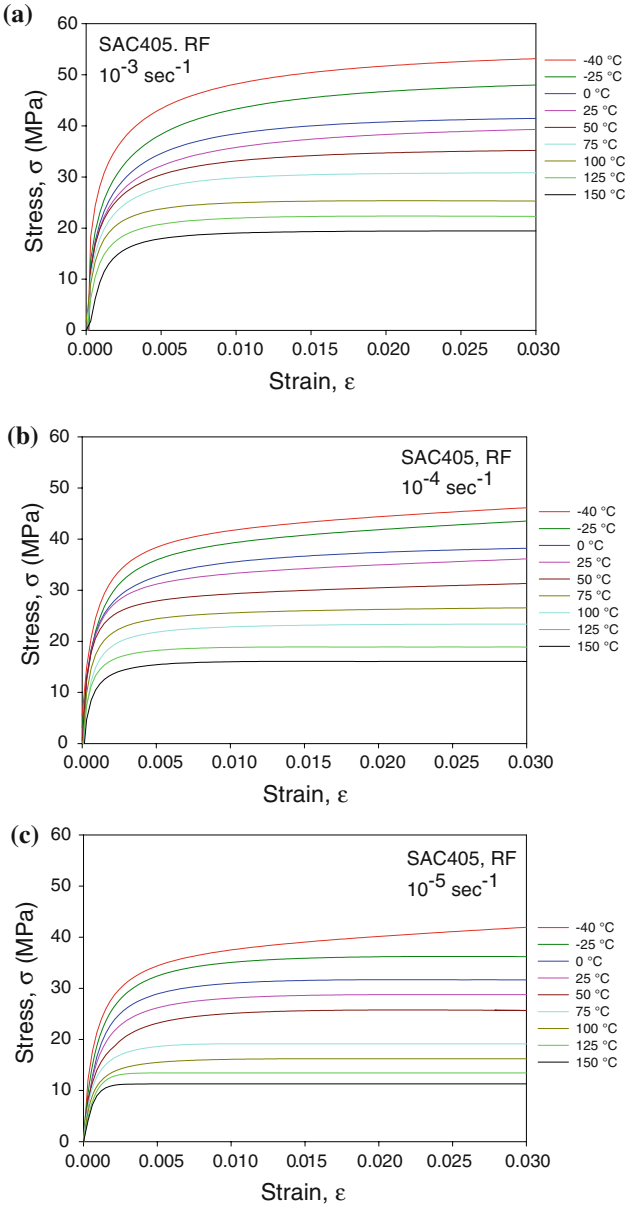

Fig. 7 SAC405 stress–strain curves at various temperatures at **a** 10^{-3} s^{-1}, **b** 10^{-4} s^{-1}, and **c** 10^{-5} s^{-1}

temperature. Similar to that of SAC alloy, the tensile properties decreased dramatically with increasing temperature. The linear models at all three strain rates are summarized in Table 3. Tensile strength follows a power law relationship with the strain rates. The power law models for Sn–Pb solder at different temperatures are summarized in Table 4. The power constants continue to increase with increasing temperature. Compared to the power constants in SAC, the Sn–Pb solder has noticeably higher constants at higher temperatures, which implies that the Sn–Pb is more strain rate sensitive at higher temperatures. The data

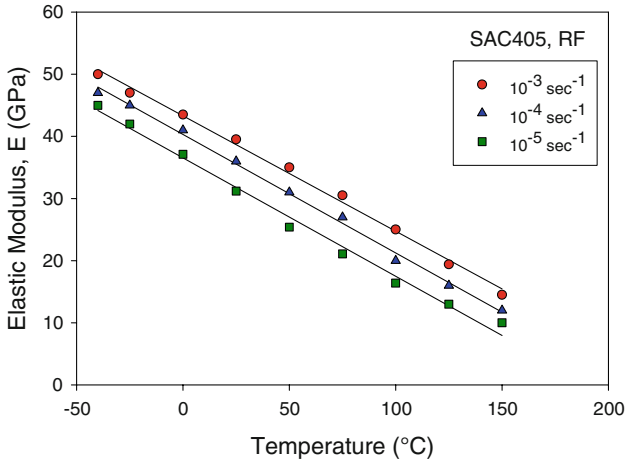

Fig. 8 SAC405 elastic modulus versus temperature at different strain rates

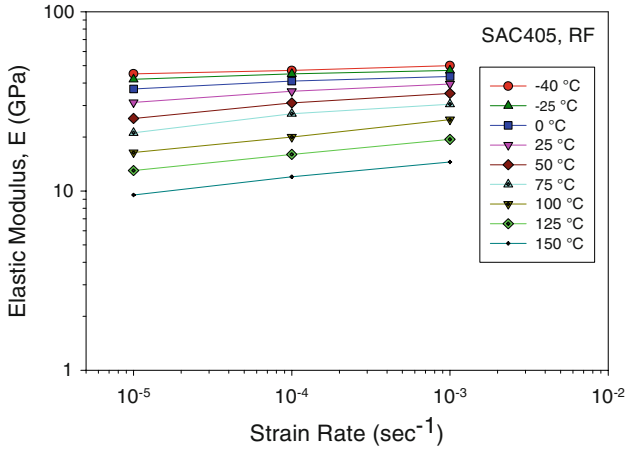

Fig. 9 SAC405 elastic modulus versus strain rate at various temperatures

show that both lead-free solder and Sn–Pb solder alloys follow a similar relationship between the tensile properties, temperature, and strain rates.

Figures 10, 11 show the comparison between Sn–Pb and SAC405, the elastic modulus of SAC405 is higher than Sn–Pb at all strain rates and temperatures. However, as shown in Fig. 11, the elastic modulus of SAC405 was more sensitive to temperature than that of Sn–Pb, and it drops faster at higher temperature than that of Sn–Pb. The strain rate dependency was similar for both alloys at lower temperature. Sn–Pb was more sensitive to strain rates at higher temperatures (Fig. 11), which may be due to the low melting temperature of Sn–Pb.

Higher temperature is believed to induce initiations of macroscopic fractures, which leads to a reduction in the tensile strength at higher temperature [1]. The elastic modulus is believed to be related to the interatomic bonds as well [1], and is negative to a power of the distance between adjacent atoms [14]. Higher temperatures will cause an increase in the distance between adjacent atoms, which will therefore lead to the reduction in the apparent elastic modulus.

The strain rate dependence is believed to be related to the strain hardening process during testing. At higher strain rates, strain hardening produces a dramatic increase in the number of dislocations and dislocation interactions in the materials. High dislocation densities will quickly increase the strength of the material.

Constitutive models

The test results show that a clear linear relationship between tensile properties and testing temperature, and a near power law relationship to strain rates were found. However, in actual solder joints, the temperature and strain rates may be random, so a constitutive model that takes into account both temperature and strain rate is needed to effectively predict the material behavior of solder alloys.

Most current reports have focused on a single variation such as linear relationship with respect to temperature, or the of power relationship with strain rate [6–9]. Shi and

Table 1 SAC405 tensile properties versus temperature at different strain rates

Strain rate (s^{-1})	Temperature range	Temperature dependence	R^2
10^{-3}	E	$E = -0.1857T + 43.313$	0.9953
	UTS	$\sigma_{UTS} = -0.1736T + 44.353$	0.9966
	YS	$\sigma_{0.2} = -0.0928T + 30.953$	0.9958
10^{-4}	E	$E = -0.1907T + 40.301$	0.9966
	UTS	$\sigma_{UTS} = -0.1659T + 39.037$	0.9992
	YS	$\sigma_{0.2} = -0.092T + 27.955$	0.9988
10^{-5}	E	$E = -0.1919T + 36.553$	0.9930
	UTS	$\sigma_{UTS} = -0.1545T + 32.79$	0.9841
	YS	$\sigma_{0.2} = -0.0983T + 24.167$	0.9907

Table 2 SAC405 tensile properties versus strain rates at various temperatures

Temperature (°C)	Elastic modulus		UTS		YS	
	E	R^2	σ_{UTS}	R^2	$\sigma_{0.2}$	R^2
−40	$58.383(\dot{\varepsilon})^{0.0229}$	0.9899	$73.581(\dot{\varepsilon})^{0.0506}$	0.9991	$45.425(\dot{\varepsilon})^{0.0379}$	0.9997
−25	$55.875(\dot{\varepsilon})^{0.0244}$	0.9831	$77.702(\dot{\varepsilon})^{0.0657}$	0.9938	$46.664(\dot{\varepsilon})^{0.0493}$	0.9915
0	$55.605(\dot{\varepsilon})^{0.0346}$	0.9786	$72.936(\dot{\varepsilon})^{0.0712}$	0.9798	$44.819(\dot{\varepsilon})^{0.0539}$	0.9689
25	$56.742(\dot{\varepsilon})^{0.0512}$	0.9851	$66.204(\dot{\varepsilon})^{0.0718}$	0.9812	$43.493(\dot{\varepsilon})^{0.0607}$	0.9832
50	$57.353(\dot{\varepsilon})^{0.0696}$	0.9807	$57.353(\dot{\varepsilon})^{0.0696}$	0.9807	$47.358(\dot{\varepsilon})^{0.0801}$	0.9871
75	$54.119(\dot{\varepsilon})^{0.0800}$	0.9632	$67.201(\dot{\varepsilon})^{0.1071}$	0.9839	$45.621(\dot{\varepsilon})^{0.0867}$	0.9748
100	$46.859(\dot{\varepsilon})^{0.0915}$	0.9989	$51.948(\dot{\varepsilon})^{0.0974}$	0.9787	$41.952(\dot{\varepsilon})^{0.0932}$	0.9609
125	$35.455(\dot{\varepsilon})^{0.0869}$	0.9995	$46.983(\dot{\varepsilon})^{0.1044}$	0.9886	$39.343(\dot{\varepsilon})^{0.0998}$	0.9677
150	$27.545(\dot{\varepsilon})^{0.0918}$	0.9963	$44.515(\dot{\varepsilon})^{0.1204}$	0.9984	$37.092(\dot{\varepsilon})^{0.1105}$	0.9631

Table 3 Sn–Pb tensile properties versus temperature at different strain rates

Strain rate (s^{-1})	Temperature range	Temperature dependence	R^2
10^{-3}	E	$E = -0.1352T + 29.875$	0.9986
	UTS	$\sigma_{UTS} = -0.2455T + 50.691$	0.9916
	YS	$\sigma_{0.2} = -0.2239T + 47.311$	0.9939
10^{-4}	E	$E = -0.134T + 26.418$	0.9952
	UTS	$\sigma_{UTS} = -0.2325T + 39.817$	0.9877
	YS	$\sigma_{0.2} = -0.2097T + 36.196$	0.9946
10^{-5}	E	$E = -0.1345T + 23.474$	0.9967
	UTS	$\sigma_{UTS} = -0.185T + 27.437$	0.9744
	YS	$\sigma_{0.2} = -0.1806T + 24.891$	0.9677

Table 4 Sn–Pb tensile properties versus strain rates at various temperatures

Temperature (°C)	Elastic modulus		UTS		YS	
	E	R^2	σ_{UTS}	R^2	$\sigma_{0.2}$	R^2
−40	$47.096(\dot{\varepsilon})^{0.0421}$	0.9999	$137.33(\dot{\varepsilon})^{0.1121}$	0.9806	$130.11(\dot{\varepsilon})^{0.1153}$	0.9946
−25	$44.665(\dot{\varepsilon})^{0.0436}$	0.9902	$136.71(\dot{\varepsilon})^{0.1254}$	0.9972	$120.06(\dot{\varepsilon})^{0.1187}$	0.9890
0	$42.013(\dot{\varepsilon})^{0.0485}$	0.9990	$140.85(\dot{\varepsilon})^{0.1432}$	0.9951	$121.01(\dot{\varepsilon})^{0.1321}$	0.9999
25	$42.206(\dot{\varepsilon})^{0.0652}$	0.9984	$135.03(\dot{\varepsilon})^{0.1619}$	0.9858	$134.78(\dot{\varepsilon})^{0.1690}$	0.9761
50	$38.044(\dot{\varepsilon})^{0.0739}$	0.9950	$126.27(\dot{\varepsilon})^{0.1776}$	0.9802	$151.21(\dot{\varepsilon})^{0.2053}$	0.9731
75	$40.109(\dot{\varepsilon})^{0.1020}$	0.9958	$148.11(\dot{\varepsilon})^{0.2179}$	0.9915	$224.23(\dot{\varepsilon})^{0.2834}$	0.9658
100	$35.133(\dot{\varepsilon})^{0.1132}$	0.9991	$141.23(\dot{\varepsilon})^{0.2458}$	0.9895	$214.58(\dot{\varepsilon})^{0.3055}$	0.9789
125	$30.500(\dot{\varepsilon})^{0.1259}$	0.9826	$144.60(\dot{\varepsilon})^{0.2768}$	0.9978	$384.44(\dot{\varepsilon})^{0.4148}$	0.9678
150	$41.274(\dot{\varepsilon})^{0.1990}$	0.9740	$364.34(\dot{\varepsilon})^{0.4447}$	0.9794	$760.28(\dot{\varepsilon})^{0.5485}$	0.9659

Pang (co-workers) have proposed the following constitutive models for eutectic Sn–Pb solder that include variables for both temperature and strain rate [4, 5]:

$$E(T,\dot{\varepsilon}) = (k_1T + k_2)\log(\dot{\varepsilon}) + (k_3T + k_4) + k_0 \quad (3)$$

$$\sigma_{\mathrm{UTS,YS}}(T,\dot{\varepsilon}) = (C_1 + C_2)[\dot{\varepsilon}]^{(C_3T+C_4)}, \quad (4)$$

where k_0–k_4 and C_1–C_4 are materials constants. The model for the elastic modulus (Eq. 3) considers both the near linear temperature effects and strain rate contribution. The UTS and YS model also consider both the effects of temperature and strain rate (Eq. 4). Shi et al. [4] used experimental data for both the temperature variable and the strain rate variable. In this study, experimental data fitted with multiple variables for both lead-free and Sn–Pb solders according to Shi's models. The data fit the models perfectly. Figure 12 illustrates the 3-D mesh fitting to the elastic modulus for SAC405, it indicates that the model

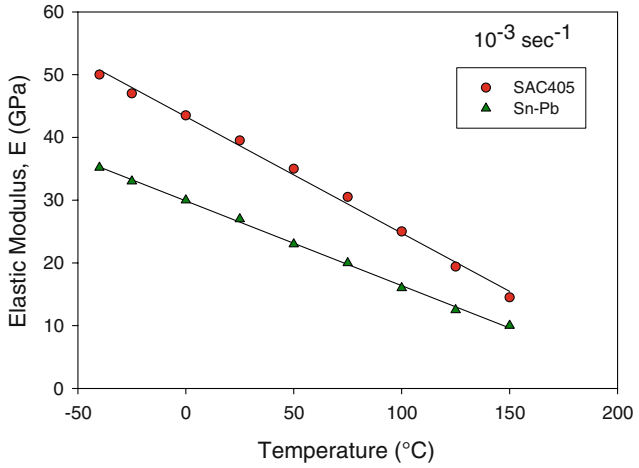

Fig. 10 Elastic modulus versus temperature for Sn–Pb and SAC405

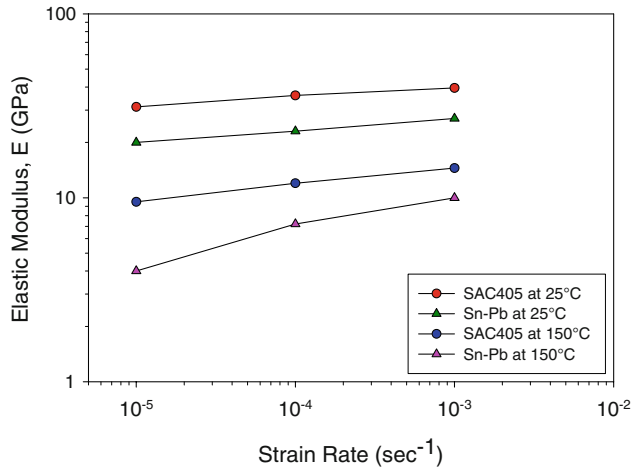

Fig. 11 Elastic modulus versus strain rate for Sn–Pb and SAC405

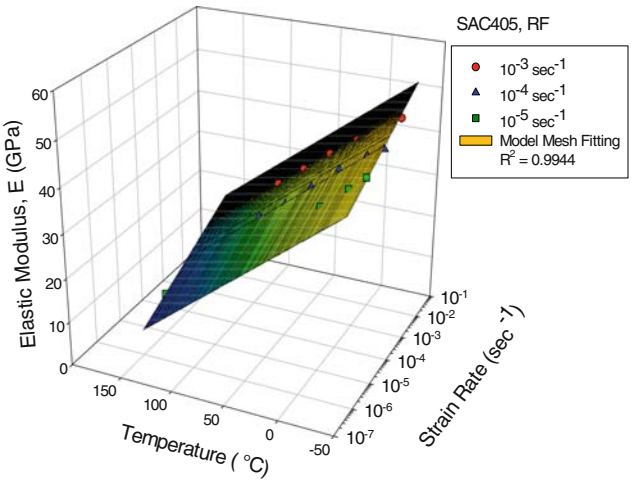

Fig. 12 Two variable fitting with constitutive model for elastic modulus of SAC405

was closely fitted, similar data fitting were also evaluated for UTS and YS. Corresponding to the multiple variables mesh fitting of tensile properties for Sn–Pb were also evaluated. The constitutive models and all the materials constants were obtained for both alloys and are summarized in Table 5. The R^2 values indicate a near perfect fit to our experimental data with the constitutive models to both lead-free and Sn–Pb solders. Figure 13 illustrates the comparison of elastic modulus of the constitutive models obtained to the experimental data for the SAC alloys. It indicates a near perfect fitting to the models.

The Shi et al.'s models were originally developed for Sn–Pb eutectic solder [4]. The data in this study proves that the constitutive models (Eqs. 3, 4) are also a good fit for SAC alloys. However, comparing with Shi et al.'s model for eutectic Sn–Pb, there are large discrepancies. Figure 14 shows comparison of the elastic constitutive models for elastic modulus between Shi et al.'s model and the model presented in this article at 10^{-3} s^{-1}. The data variation may be caused by the differences of specimen preparation (Shi's specimens were machined), specimen geometry (Shi's are cylindrical) and size (Shi's dimensions are 30 mm in gage length and 6 mm in diameter). It is also possible, as our past research shows that the room temperature aging effects may also contribute to these inconsistencies [13]. Shi et al.'s specimen was aged at 60 °C for 24 h to reduce the machining residual stress. As explained previously, the machining method is not suitable for bulk specimen preparation for solder alloys due to the dramatic heating effects generated during the machining process. The testing conditions of Shi et al.'s room temperature aging periods were also unclear.

Summary and conclusions

Due to the CTE mismatch and variations in the operating conditions, solder joints will experience constant stresses at different strain rates and temperatures, and are extremely sensitive to strain rates and temperature changes due to their high homologous temperatures. In this study, the effects of strain rates and temperature on the tensile properties of lead-free solder and Sn–Pb solders were investigated. The effects of room temperature aging on the tensile properties was considered and minimized by aging the specimens at room temperature for up to 10 days to reach a relatively stable region based previous studies.

Constitutive models were obtained for both SAC405 and Sn–Pb solder alloys by fitting experimental data with Shi et al.'s models. The constitutive models provided a near perfect fit with the experimental data. Using the new constitutive models, the mechanical properties of solder alloys can be predicted for any testing conditions by

Table 5 Constitutive models of tensile properties at various temperature and strain rates for SAC405 and Sn–Pb eutectic solders

Solder type	Constitutive models	R^2
SAC405	$E(T,\dot{\varepsilon}) = (1.35\text{E}{-}03T + 3.20)\log(\dot{\varepsilon}) - 0.17701T + 55.57$	0.9944
	$\sigma_{\text{UTS}}(T,\dot{\varepsilon}) = (-0.2241T + 70.98)[\dot{\varepsilon}]^{(2.00\text{E}-04T+0.06766)}$	0.9941
	$\sigma_{\text{YS}}(T,\dot{\varepsilon}) = (-0.7103T + 45.59)[\dot{\varepsilon}]^{(2.76\text{E}-04T+0.05578)}$	0.9890
Sn–Pb eutectic	$E(T,\dot{\varepsilon}) = (-1.33\text{E}{-}04T + 2.20)\log(\dot{\varepsilon}) - 0.14281T + 36.12$	0.9964
	$\sigma_{\text{UTS}}(T,\dot{\varepsilon}) = (-0.4197T + 132.83)[\dot{\varepsilon}]^{(4.92\text{E}-04T+0.1403)}$	0.9890
	$\sigma_{\text{YS}}(T,\dot{\varepsilon}) = (0.7689T + 132.03)[\dot{\varepsilon}]^{(1.55\text{E}-03T+0.14768)}$	0.9655

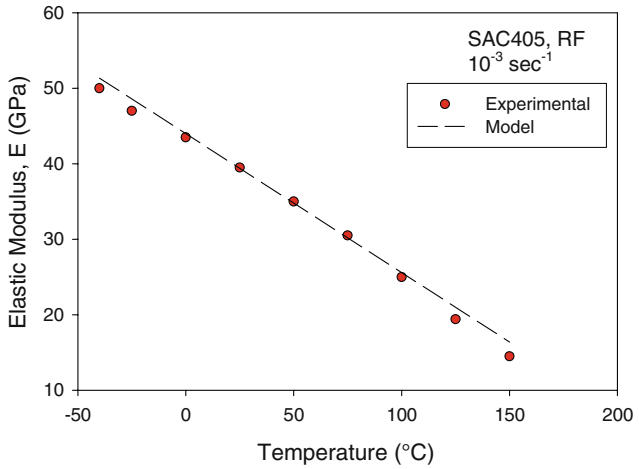

Fig. 13 SAC405 elastic modulus experimental versus constitutive model

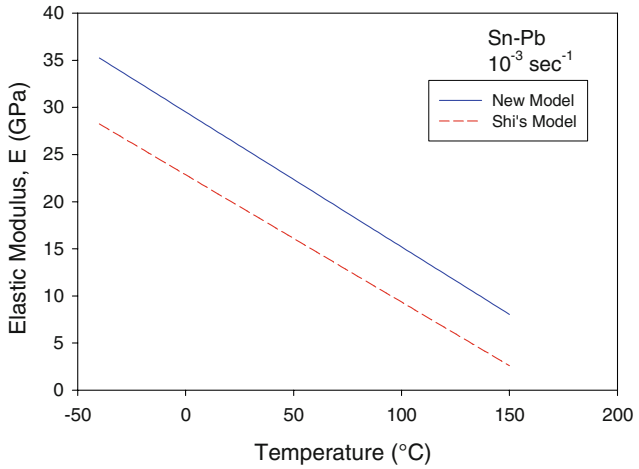

Fig. 14 Comparison of the constitutive models with Shi's model

applying both variables of strain rate and temperature. This data provided the baseline for finite element analysis by which the mechanical properties of the alloys at other conditions could be predicted. The data also shows a large deviation between our models and Shi et al.'s data for Sn–Pb eutectic solder. These discrepancies may be caused by the differences in specimen preparation and specimen dimensions. Room temperature aging effects may also have contributed to this discrepancy.

References

1. Hertzberg RW (1996) Deformation and fracture mechanics of engineering materials, 4th edn. Wiley, New York
2. Jones WK, Liu Y, Zampino MA, Gonzalez G, Shah M (1997) Design and reliability of solders and solder interconnections. TMS, Warrendale
3. Jones WK, Liu Y, Zampino MA, Gonzalez G (1997) In: Advanced microelectronics, pp 30–34
4. Shi XQ, Zhou W, Pang HLJ, Wang ZP (1999) J Electron Packag 121(3):179
5. Pang HLJ, Wang YP, Shi XQ, Wang ZP (1998) IEEE/CPMT electronics packaging technology conference, pp 184–189
6. Nose H, Sakane M, Tsukada T, Nishimura H (2003) J Electron Packag 124:59
7. Plumbridge WJ, Gagg CR (1999) J Mater Sci Mater Electron 10:461
8. Lang R, Tanaka H, Munegata O, Taguchi T, Narita T (2005) Mater Charact 54:223
9. Dai LH, Lee SR (2001) Proceeding of the ASME InterPACK'05, pp 307–313
10. Raeder CH, Mitlin D, Messler RW (1998) J Mater Sci 33(18):4503. doi:10.1023/A:1004439931547
11. El-Rehim AFA (2008) J Mater Sci 43(4):1444. doi:10.1007/s10853-007-2312-4
12. Ma H, Suhling JC (2009) J Mater Sci 44(5):1141. doi:10.1007/s10853-008-3125-9
13. Ma H, Suhling JC, Lall P, Bozack MJ (2006) Proceeding of the 56th electronic components and technology conference (ECTC), pp 849–864, San Diego, CA, May 30–June 2, 2006
14. Gilman JJ (1969) Micromechanics of flow in solids. McGraw-Hill, New York